JACS
JOURNAL OF THE AMERICAN CHEMICAL SOCIETY

Article

pubs.acs.org/JACS

Coupling Strategies to Enhance Single-Molecule Magnet Properties of Erbium–Cyclooctatetraenyl Complexes

Jennifer J. Le Roy,[†] Liviu Ungur,[‡] Ilia Korobkov,[†] Liviu F. Chibotaru,[‡] and Muralee Murugesu*[,†]

[†]Department of Chemistry, University of Ottawa, 10 Marie Curie, Ottawa, Ontario K1N 6N5, Canada

[‡]Theory of Nanomaterials Group and INPAC Institute for Nanoscale Physics and Chemistry, Katholieke Universiteit Leuven, Celestijnenlaan, 200F, 3001 Leuven, Belgium

Supporting Information

ABSTRACT: Two different coupling strategies were employed to create Er^{III} single-molecule magnets (SMMs) using high blocking temperature mononuclear precursors. The magnetic properties of three lanthanide–COT complexes, $[Er^{III}_2(COT'')_3]$ (**1**) (COT'' = 1,4-bis(trimethylsilyl)cyclooctatetraenyl dianion) and $K_2(THF)_4[Ln^{III}_2(COT)_4]$ (Ln = Gd (**2**), Er (**3**); THF = tetrahydrofuran, COT = cyclooctatetraenyl dianion), are reported. Both Er^{III} complexes behave as SMMs and exhibit magnetic hysteresis at 12 K in solid state. In solution compound **1** exhibits hysteresis up to 14 K. Ac susceptibility data indicates a 100 s blocking temperature of 12.5 and 12.9 K for $[Er^{III}_2(COT'')_3]$ and $K_2(THF)_4[Er^{III}_2(COT)_4]$, respectively. Both Er^{III} dimers display enhanced SMM properties over their mononuclear analogues due to their linear structure and strictly axial anisotropy. A 4 K increase in the magnetic blocking temperature of $[Er^{III}_2(COT'')_3]$ over the double-decker analogue is attributed to an additional mechanism of magnetization blocking arising from exchange coupling between Er^{III} ions.

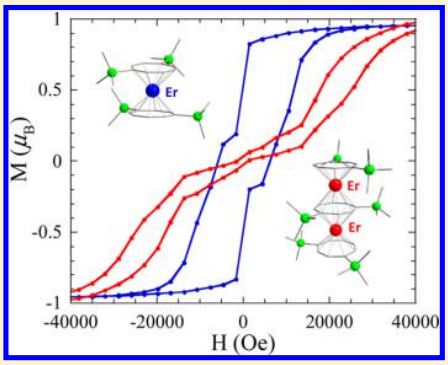

1. INTRODUCTION

Single-molecule magnets (SMMs) are molecular scale nanomagnets with tremendous application potential for information storage and molecular spintronics.[1] These highly desirable applications are dependent on raising the blocking temperature, i.e., the temperature limit where magnet-like behavior is observed. As such, significant attention has been given to understanding the origin of magnetization and how different metal ions and crystal fields influence spin reversal.[2] Hundreds of multimetallic complexes display SMM behavior, however it is interesting that some of the highest reported blocking temperatures are lanthanide complexes composed of a single metal ion.[3] The success of lanthanide single-ion magnets (SIMs) results from the combination of a large number of unpaired electrons, and the large spin–orbit coupling particularly found in late 4f elements. Fine-tuning the crystal field and local symmetry around individual lanthanide ions has been a successful strategy to increase the blocking temperatures of SIM's. Liu et al. recently reported a Dy^{III} complex with quasi-D_{5h} geometry that exhibits a SIM blocking temperature of 11 K.[3e] The success of the complex resulted from the high local symmetry around the spin carrier which prevents certain crystal field parameters that can result in quantum tunneling of the magnetization (QTM).[3e] Further fine-tuning of local symmetry could no doubt result in SIMs with higher blocking temperatures, however, such a strategy has a finite ceiling for improvement. Here, we establish that increasing the total spin of an SMM while also considering local symmetry is an effective approach to increasing blocking temperature.

In order to significantly increase the blocking temperature of lanthanide SMMs, the total spin of the molecule needs to increase, therefore the number of paramagnetic ions need to increase in a system. Multinuclear lanthanide SMMs are numerous, but only one complex has surpassed the blocking temperature of the best performing SIMs.[4a] This is due to the poor radial extension of the 4f orbitals which results in week exchange coupling between lanthanide ions. Therefore, multinuclear lanthanide SMMs usually display predominant single-ion relaxation dynamics. Several strategies have been explored to increase exchange coupling between lanthanide ions including the use of heavier elements with more diffuse orbitals[5] as well as bridging radicals[4] as potential and efficient superexchange pathways. The radical approach has been the most successful in obtaining strong exchange coupling constants between two lanthanide ions thanks to the presence of an unpaired electron on the ligand, however, extending this methodology to larger molecules involving multiple metal centers/radicals is synthetically very difficult and has led to limited application of this approach.

We recently reported a building block strategy to create triple decker bimetallic lanthanide SMMs using planar aromatic COT''^{2-} ligands (COT'': 1,4-bis(trimethylsilyl)-

Received: March 7, 2014
Published: May 7, 2014

   dx.doi.org/10.1021/ja5022552 | J. Am. Chem. Soc. 2014, 136, 8003–8010

cyclooctatetraenyl dianion).[6] The use of a bridging COT''^{2-} ligand provides a delocalized superexchange pathway ideal for promoting magnetic interaction between lanthanide ions, as demonstrated in $[Dy^{III}_2(COT'')_3]$, which exhibited a weak $Dy^{III}-Dy^{III}$ covalent bond.[6] Magnetically both $[Dy^{III}_2(COT'')_3]$ and the mononuclear starting building block, $[Dy^{III}(COT'')_2]^-$, display SMM properties.[6] The benefit of a building block strategy allows for fine-tuning of the mononuclear unit, therefore, in extension to this work we investigated both symmetry effects and the use of different metals in Ln^{III}–COT based sandwich complexes.[3a,b,6,7] This systematic approach led to the formation of $[Er^{III}(COT)_2]^-$ and $[Er^{III}(COT'')_2]^-$ SMM complexes which display high single-ion blocking temperatures of 10 and 8 K, respectively.[3a,b] Therefore, $[Er^{III}(COT)_2]^-$ based sandwich complexes are ideal candidates to employ as building blocks in pursuit of higher blocking temperature SMMs. With this in mind, we investigated two different strategies to coupling aforementioned SIMs, specifically focusing on linear complexes to maximize uniaxial anisotropy, with varying distance between building block units.

Herein we present the synthesis, structure and magnetic properties of three Ln^{III}–COT multidecker complexes, $[Er^{III}_2(COT'')_3]$ (COT'' = 1,4-bis(trimethylsilyl)-cyclooctatetraenyl dianion) (**1**), $K_2(THF)_4[Ln^{III}_2(COT)_4]$ (Ln = Gd (**2**), Er(**3**)), and a magnetic comparison with their respective mononuclear precursors.

2. EXPERIMENTAL SECTION

General Synthetic Considerations. Unless specified otherwise, all manipulations were performed under an inert atmosphere using standard Schlenk or glovebox techniques. Glassware was oven-dried (120 °C, 6 h) before use. Hexanes, pentane, cyclopentane, toluene, and tetrahydrofuran (THF) were dried using activated alumina and stored over 3 Å molecular sieves. All chemicals were purchased from Thermofisher Scientific or Strem and used without further purification. The $[Li_4(COT'')_2(THF)_4]$ was synthesized using a previously published procedure.[8] IR data were collected on a Varian 640 FT-IR spectrometer. ^{1}H spectra were recorded on a 300 MHz Bruker Advance spectrometer at room temperature (21–23 °C). THF-d_8 was dried over sodium metal for 24 h, distilled, and then stored over 3 Å molecular sieves. Toluene-d_8 was dried using activated alumina and 3 Å molecular sieves.

Synthesis of $[Er^{III}_2(COT'')_3]$ (1). $ErCl_3$ (0.113 g, 0.414 mmol) was added to $[Li_4(COT'')_2(THF)_4]$ (0.495 g, 0.621 mmol) dissolved in THF (5 mL) in a 20 mL scintillation vile. The resulting solution stirred for 36 h at room temperature, after which the solvent was removed *in vacuo*. The product was extracted with hot toluene (5 mL) before subsequent filtration through a fine-fritted funnel. The solution was concentrated and then cooled to −37 °C. After 5 h an orange precipitate appeared. The solid was filtered and washed with hexanes, yielding $[Er^{III}(COT'')_2]Li(THF)_4$, as a orange crystalline powder (220 mg, 52%). Selected IR data (cm^{-1}): 2951 (br), 2887 (m), 1444 (w), 1243 (s), 1214 (w), 1051 (s), 984 (w), 934 (m), 832 (s), 747 (m), 717 (m), 679 (w), 634 (w). Complex **1** was produced from a reaction of $[Er^{III}(COT'')_2]Li(THF)_4$ (0.200 g, 0.194 mmol) with $CoCl_2$ (0.013 g, 0.097 mmol). The reagents were refluxed in toluene (5 mL) for 5 h. Co^0 was removed via filtration as a black precipitate using a fine fritted funnel. The remaining solution was concentrated to an amber oil from which large block crystals of **1** were grown by the addition of 0.5 mL of cyclopentane at −35 °C (20% yield). Individual block crystals were picked out of the oil and recrystallized from cyclopentane. Isolated X-ray diffraction quality crystals are air and moisture sensitive. Selected IR data for **1** (cm^{-1}): 2999 (w), 2957 (br), 2900 (m), 1450 (br), 1403 (w), 1247 (s), 1049 (m), 978 (w), 933 (w), 837 (s), 748 (m), 721 (w), 688 (w), 634 (w). ^{1}H NMR (300 MHz, toluene-d_8): δ 7.12 (br s), 7.04 (br s), 7.00 (br s), 2.11 (br s), 0.11 (br s) ppm. UV–vis (0.3 mM cyclopentane): $\lambda_{max}(\varepsilon)$ = 273(1.035).

Synthesis of $K_2(THF)_4[Gd^{III}_2(COT)_4]$ (2). In a 20 mL scintillation vile, freshly cut K^0 (164 mg, 0.42 mmol) was added to THF (10 mL), and the solution was cooled to −37 °C in a drybox freezer. 1,3,5,7-Cyclooctatetraene (0.192 mL, 0.2 mmol) was added, and the resulting solution remained at −37 °C for 2 days without stirring. $GdCl_3$ (290 mg, 0.11 mmol) was added, and the resulting mixture was slowly warmed to room temperature. The mixture was vigorously stirred for 3 h at room temperature and then filtered through a fine fritted funnel containing Celite. The resulting solution was concentrated, and single crystals of **2** suitable for X-ray diffraction were grown at −37 °C with 10% v/v addition of pentane after 1 week (yield 381 mg, 63%). Selected IR data for **2** (cm^{-1}): 2969 (w), 2922 (br), 1850 (w), 1457 (m), 1316 (w), 1262 (m), 1099 (w), 1025 (w), 889 (w), 799 (m), 743 (m). ^{1}H NMR (300 MHz, THF-d_8) δ 3.90 (br s), 1.80 (br s), −0.05 (br s) ppm.

Synthesis of $K_2(THF)_4[Er^{III}_2(COT)_4]$ (3). Complex **3** was synthesized in the analogous manor to **2** where freshly cut K^0 (164 mg, 0.42 mmol) was added to THF (10 mL), and the solution was cooled to −37 °C in a drybox freezer. 1,3,5,7-Cyclooctatetraene (0.192 mL, 0.2 mmol) was added, and the resulting solution remained at −37 °C for 2 days without stirring. $ErCl_3$ (274 mg, 0.11 mmol) was added, and the resulting mixture was slowly warmed to room temperature. The mixture was vigorously stirred for 3 h at room temperature and then filtered through a fine fritted funnel containing Celite. The resulting solution was concentrated and single crystals of **3**, suitable for X-ray diffraction, were grown at −37 °C with 10% v/v addition of pentane after 1 week (yield 405 mg, 66%). Selected IR data for **3** (cm^{-1}): 3005 (w), 2925 (br), 1840 (w), 1456 (m), 1319 (w), 1262 (w), 1099 (w), 1058 (w), 893 (s), 799 (m), 743 (m). ^{1}H NMR (300 MHz, THF-d_8) δ 5.39 (br s), 4.04 (br s), 1.88 (br s) ppm.

X-ray Crystallography. Large single crystals of **1** were grown from an amber oil at −37 °C, as described above, and were washed thoroughly with cold cyclopentane before use. Large single crystals of **2** and **3** were grown from a concentrated THF/pentane solution at −37 °C and washed thoroughly with hexanes before use. For **1**–**3**, a suitable prism-shaped crystal was mounted in inert oil and transferred to the cold gas stream of the diffractometer. Unit cell measurements and intensity data were collected at 200 K on a Bruker-AXS SMART 1 k CCD diffractometer using graphite monochromated MoK_α radiation (λ = 0.71073 Å). The data reduction included a correction for Lorentz and polarization effects, with an applied multiscan absorption correction (SADABS).[9] The crystal structures were solved and refined using the SHELXTL[10] program suite. Direct methods yielded all non-hydrogen atoms, which were refined with anisotropic thermal parameters. All hydrogen atom positions were calculated geometrically and were riding on their respective atoms. The crystal structures have been deposited at the Cambridge Crystallographic Data Centre and allocated the deposition numbers CCDC 974992, 974994 and 974993.

Magnetic Measurements. Magnetic susceptibility measurements for **1**–**3** were obtained using a Quantum Design SQUID magnetometer MPMS-XL7 operating between 1.8 and 300 K for direct current (dc) applied fields ranging from −7 to 7 T. Dc analyses were performed on polycrystalline samples sealed in a polyethylene membrane (prepared in an inert atmosphere) under a field ranging from 0 to 7 T and temperatures between 1.8 and 300 K. Ac susceptibility measurements were carried out under an oscillating ac field of 3 Oe and ac frequencies ranging from 1 to 1500 Hz. Magnetization data were collected at 100 K to check for ferromagnetic impurities that were absent in all samples. Diamagnetic corrections were applied for the sample holder and the core diamagnetism from the sample (estimated with Pascal constants).

Ab Initio Calculations. All calculations were done with MOLCAS 7.8 and are of CASSCF/RASSI/SINGLE_ANISO type. The entire molecule was computed ab initio, while neighboring Er ions were computationally modeled by diamagnetic Lu. Two basis set approximations have been employed: 1, small, and 2, large; Table S2 shows the contractions of the employed basis sets for all elements. Active space of the CASSCF method includes the 11 electrons from

dx.doi.org/10.1021/ja5022552 | J. Am. Chem. Soc. 2014, 136, 8003–8010

the last shell spanning the 7 orbitals (4f orbitals of the Er^{III} ion). On the basis of the resulting spin−orbital multiplets the SINGLE_ANISO program computed local magnetic properties (g-tensors, main magnetic axes, local magnetic susceptibility, etc.) Further, the exchange and dipolar interactions between magnetic centers were computed by the POLY_ANISO program.

3. RESULTS AND DISCUSSION

Synthesis and Structural Analysis. Complexes **1**−**3** were synthesized with minor modifications to either previously published procedures or a structurally analogous lanthanide complex.[6,11] The synthesis of **1** was inspired from Edelman and co-workers' meticulous development of Ln−COT″ chemistry.[11b,c] The crystallization parameters for **1**−**3** are provided in the Supporting Information. The structure of **1** crystallizes in a tetragonal $I\bar{4}$ space group and is composed of two Er^{III} ions sandwiched between three COT″ rings, each bound η^8 to the metal as represented by the average $Er^{III}-C_{COT''}$ distance of 2.39 Å (Figures 1, S1−S2). The structure of **1** is near linear

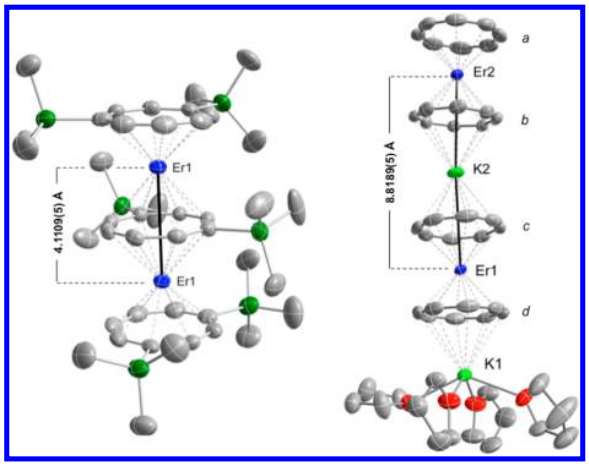

Figure 1. Molecular X-ray structures of **1** (left) and **3** (right) with thermal ellipsoids drawn at 50% probability. Hydrogen atoms were omitted for clarity. Color code; Blue (Er^{III}), dark green (Si), light green (K), red (O), gray (C). Selected distances [Å] and angles [°]: (**1**) Er1−Er1 4.11, Er1−COT″$_{centroid}$−Er1 (bridging COT″ centroid) 175.65, Er1−COT$_{centroid}$ (average for exterior COT″ decks) 1.75, Er1−COT$_{centroid}$ (average for interior COT″ decks) 2.06; (**3**) Er1−Er2 8.82, Er2−K2 4.43, K2−Er1 4.42, K1−Er1 4.51, K1−O (average) 2.70, Er1−K2−Er2 169.57, K1−Er1−K2 179.34, Er2−COT (average) 2.58 (*a* deck) and 2.66 (*b* deck), Er1−COT (average for *a* and *b* decks) 2.61, K1−O (average) 2.70.

with an Er1−COT$_{centroid}$−Er1 angle of 175.65°. The Er1−Er1 distance of 4.11 Å is closer than analogous Dy_2 (4.14 Å) and Gd_2 (4.21 Å) complexes, consistent with Ln contraction. Uneven charge donation between terminal and bridging COT″ rings are reflected by average $Er^{III}-C_{COT}$ (terminal) and $Er^{III}-C_{COT}$ (bridging) distances of 2.53 and 2.76 Å, respectively. Similar behavior was observed in the analogous Dy^{III} complex where DFT calculations established this difference is due to uneven ligand donation; the central COT″ ring donation is shared between two metal ions, whereas the terminal COT″ rings donation is directed toward only one metal center.[6]

Complexes **2** and **3** are isostructural, each crystallizing in a triclinic *P*-1 space group. The molecular structure of **2** is located in the Supporting Information as well as a table containing the structural details of **1**−**3** (Table S1, Figures S3−S4). As **2** and **3** are isostructural, the structure of the Er analogue, complex **3**, will be described (Figures 1 right, S3 right). Complex **3** has a tetralayer sandwich architecture, composed of two $[Er^{III}COT_2]^-$ units which sandwich a K ion bound η^8 to both units. An additional $K(THF)_4$ countercation is bound η^8 through the K to one COT ring as reflected in the average K1−$C_{COT(d)}$ distance of 3.20 Å. The near linear structure of **3** is illustrated by Er2−K2−Er1 and K2−Er1−K1 angles of 169.57° and 179.35°, respectively. The Er−Er distance of 8.82 Å is significantly longer than in **1** (4.11 Å). Uneven charge donation is apparent in Er2 (Er2−C_{COT} average distance for decks *a* and *b* is 2.58 and 2.66 Å, respectively) as the outer COT ring (deck a) is only bound to the Er ion, whereas the inner COT (deck b) is bound to both Er and K ions. In the case of Er1, the Er1−C_{COT} average distance is more symmetrical for decks *c* and *d* (2.61 Å) as both COT decks are bound to Er1 and K ions (K1 for deck *d* and K2 for deck *c*). These slight variations in the coordination environment are expected to influence the overall magnetic properties of the complexes (*vide infra*).

Magnetic Properties. We recently described the magnetic properties of both $[Er^{III}COT_2]^-$ and $[Er^{III}(COT'')_2]^-$ building block units, in which magnetic blocking temperatures of 10 and 8 K were reported, respectively.[3a,b] Our current objective is to enhance the magnetic properties of these complexes by increasing spin through dimerization, while maintaining strictly axial anisotropy. Complexes **1** and **3** are ideal candidates due to their linearity and high axial symmetry around the spin centers. Complex **1** has a much shorter Er−Er distance than **3** (4.11 vs 8.12 Å), therefore a stronger magnetic interaction between Er^{III} ions is expected in **1**. The bridging potassium ion (K2) acts as a diamagnetic spacer between the two highly anisotropic $[Er^{III}COT_2]^-$ SIMs in **3**. However, the removal of the trimethylsilyl groups leads to a higher symmetry environment around the Er ions thus influences on the orientation of the magnetic axis. This was proven essential to the strong magnetic performance of the $[Er^{III}COT_2]^-$ monomer.[3b] To evaluate the two different coupling approaches with varying distance between Er^{III} ions, the magnetic properties of **1** and **3** were investigated using a SQUID magnetometer and compared to their respective monomer building blocks.

The dc magnetic susceptibility of **1**−**3** was measured on crushed polycrystalline samples sealed in an inert atmosphere between the temperature range of 1.8 and 300 K and a 0.1 T applied dc field (Figure 2). The magnetic properties of **1** were additionally investigated in a 4 mM cyclopentane solution to probe any intermolecular magnetic interactions. The solid-state room temperature χT product of 22.45 $cm^3{\cdot}K{\cdot}mol^{-1}$ (**1**) and 22.54 $cm^3{\cdot}K{\cdot}mol^{-1}$ (**3**) are in good agreement with the theoretical value of 22.96 $cm^3{\cdot}K{\cdot}mol^{-1}$ for two non-interacting Er^{III} ($^4I_{15/2}$, $S = 3/2$, $L = 6$, $g_J = 6/5$) ions. Upon decrease of the temperature the χT product remains fairly constant down to 150 K for **1** and below which a gradual decrease can be seen. Further sharp decrease can be observed below 50 K to reach a minimum value of 0.55 $cm^3{\cdot}K{\cdot}mol^{-1}$ a 1.8 K. Such negative deviation of the χT product can arise from a combination of several factors such as intramolecular antiferromagnetic interactions, depopulation of the excited states, crystal field effects with significant magnetic anisotropy, and/or intermolecular interations.[12] To rule out any intermolecular interactions we performed frozen solution measurement in 4 mM cyclopentane for **1** in the 1.8−100 K temperature range. The χT product again shows a steep drop at low temperatures

dx.doi.org/10.1021/ja5022552 | J. Am. Chem. Soc. 2014, 136, 8003−8010

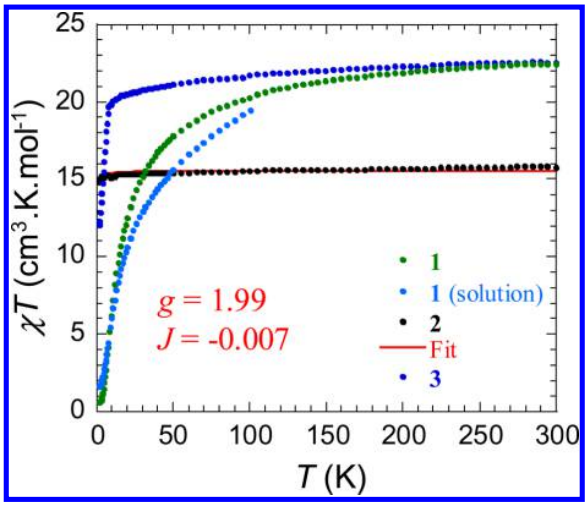

Figure 2. Solid-state temperature dependence of the χT product under 0.1 T for complex **1** (green circle), **2** (black circle), and **3** (blue circle), and 4 mM solution of **1** (light-blue circle), with χ being the molar susceptibility per dinuclear complex defined as M/H.

reaching a minimum value of 1.62 $cm^3 \cdot K \cdot mol^{-1}$, thus confirming the low temperature decrease is not due to intermolecular influence.

In the case of compound **3** the χT product remains constant down to 20 K followed by a very sharp decrease to reach a minimum value of 12.05 $cm^3 \cdot K \cdot mol^{-1}$ at 1.8 K. Such overall behavior is reminiscent of our recently reported highly anisotropic mononuclear $[Er(COT)_2]^-$ complex.[3b] Therefore, it is reasonable to assume in this case that the intramolecular interactions are expected to be weak as these Er^{III} units are separated (Er^{III}–Er^{III} distance of 8.82 Å) by the bridging K counterion, although it was not possible to quantify the coupling strength by fitting the susceptibility data through Kambe's coupling method due to the highly anisotropic nature of Er^{III} ions. Therefore, to approximate the strength of the Er^{III}–Er^{III} interaction in this system, compound **2** was synthesized and analyzed to provide an ideal isotropic model.

The room temperature χT value of 15.79 $cm^3 \cdot K \cdot mol^{-1}$ for **2** is in good agreement with the theoretical value of 15.76 $cm^3 \cdot K \cdot mol^{-1}$ for two non-interacting Gd^{III} ($^8S_{7/2}$, $S = 7/2$, $L = 0$, $g = 2$) ions. Upon decreasing the temperature the χT product remains constant with a slight decrease below 10 K to reach a minimum value of 14.30 $cm^3 \cdot K \cdot mol^{-1}$ at 1.8 K. The low temperature decrease is primarily due to intramolecular weak antiferromagnetic coupling between isotropic Gd^{III} ions. To quantify the strength of the Gd^{III}–Gd^{III} interaction, application of the van Vleck equation to the Kambe's vector coupling method was calculated using the isotropic spin Hamiltonian $H = -JS_a \cdot S_b$ with $S_a = S_b = 7/2$, which was used to fit the variation of the χT vs T data. The best fit parameters obtained are $J = -0.007(4)$ cm^{-1} and $g = 1.99(1)$ for **2**. The small J value is a consequence of the large Gd^{III}–Gd^{III} distance of 8.93 Å, in contrast, much stronger magnetic coupling is observed in the Gd^{III} analogue of **1** with $J = -0.448$ cm^{-1}, and this is most likely due to the closer Gd^{III}–Gd^{III} distance of 4.21 Å.[6] In comparison, $J = -0.448$ cm^{-1} is as expected much lower than reported for radical bridged Gd dimers[4] but comparable or slightly higher than Gd_2 coordination compounds.[2b] These results clearly suggest that in compound **3** the Er^{III} ions might behave as a weakly coupled system thus the overall magnetic behavior would resemble that of the reported $[Er(COT)_2]^-$ SIM, whereas in **1** the interactions between Er^{III} ions are non-negligable.[3b]

To confirm magnetic anisotropy in **1**–**3**, field-dependent magnetization measurements (M vs H) and reduced magnetization studies were performed (Figures S5–S7). Below 7 K there is a sinusoidal character observed in both complexes **1** and **3** at applied fields <2 T. Such a feature is generally attributed to interactions between highly anisotropic magnetic ions.[13] In **1** and **3** intramolecular metal centers are separated by 4.1 and 8.82 Å, respectively; therefore the occurring weak coupling between the Er^{III} ions most likely influences the shape and the positioning of these sinusoidal curves. Such behavior was observed in the Dy^{III} analogue of **1** as well as in a weakly coupled $\{Dy_2\}$ complex which exhibits intramolecular entanglement.[1f] The nonsaturation as well as the nonsuperimposition of iso-temperature lines in the M vs H/T data confirms the presence of significant magnetic anisotropy in **1** and **3**. The M vs H data for **2** displays a rapid and steady increase in the magnetization at 1.8 K with near saturation under 7 T. The superimposition of iso-temperature lines in the M vs H/T data is expected for isotropic Gd^{III} ions.

To investigate the blocking of the magnetization, magnetic hysteresis measurements were performed on **1** and **3** between fields of 5 and −5 T. To directly compare the magnetic blocking of **1** and **3** to their mononuclear analogues, respective sweep rates of 0.0022 and 0.0018 $T \cdot s^{-1}$ were employed, consistent with the previous reports (Figure 3).[3a,b]

Complex **1** displays clear hysteresis at 1.8 K with a coercivity at $M = 0$ Oe. Interestingly no step in the hysteresis appears at $H = 0$ in contrast to the monomer.[3a] Additionally, distinct steps appear at ~ ±15 kOe most likely arising from an intramolecular antiferromagnetic interaction between Er^{III} ions.[1f,14] Upon raising the temperature, clear coercivity at $H = 0$ is observed up until 7 K and *s*-shaped hysteresis loops remain open until 12 K (Figures 2, S8). This signifies a 4 K increase in the magnetic blocking temperature in comparison to the mononuclear analogue.[3a] The substantial increase is surprising due to the antiferromagnetic nature of the Er–Er interaction as demonstrated in the χT plot. This is most likely due to the fact that the magnetic moments of the Er^{III} ions are not fully compensated in the case of antiferromagnetic coupling. As a result, we see the blocking of the small uncompensated magnetic moment.

To probe any intermolecular influence on the hysteresis of **1**, solution measurements were performed under identical conditions. At 1.8 K the hysteresis of **1**, measured as a bulk solid and a 4 mM frozen solution in cyclopentane, show near identical behavior (Figure S9), therefore distinct steps at ~ ±15 kOe are molecular in origin and not the result of intermolecular interactions. Solution studies reveal slight improvement in the hysteresis, where openings at $H \neq 0$ are observed up until 14 K possibly due to the dilution of intermolecular antiferromagnetic interactions (Figure S10). This high temperature for blocking of the magnetization clearly shows how highly anisotropic Er^{III} ions can exhibit a remarkable performance when subjected to appropriate crystal field.

Complex **3** displays radically different behavior than **1**. At a fixed sweep rate of 0.0018 $T \cdot s^{-1}$ and at 1.8 K the appearance of a clear butterfly shape hysteresis is observed in **3** with openings at $H \neq 0$. Upon raising the temperature, openings in the hysteresis narrow and then close above 12 K (Figures 3, S11). In comparison, $[Er^{III}(COT)_2]^-$ displays clear hysteresis and remanance at $M = 0$ Oe up to 10 K. The increase in the

dx.doi.org/10.1021/ja5022552 | J. Am. Chem. Soc. 2014, 136, 8003–8010

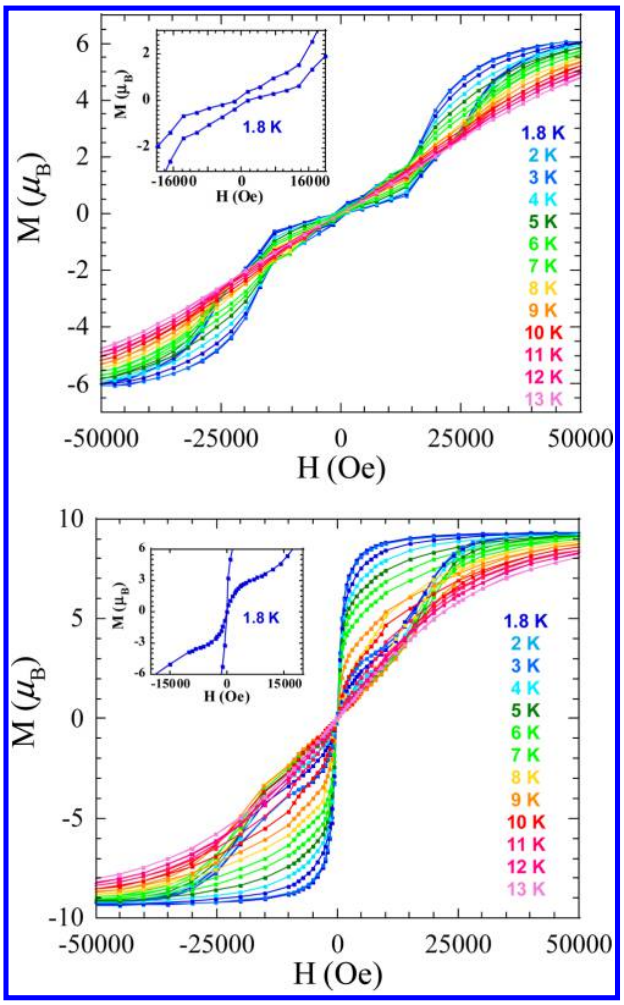

Figure 3. Magnetic hysteresis of **1** (top) and **3** (bottom) with average respective sweep rates of 0.0022 and 0.0018 T·s^{-1}, respectively. Insets: Zoomed in hysteresis loop at 1.8 K for **1** and **3**.

blocking temperature of **3** over $[Er^{III}(COT)_2]^-$ is primarily due to single-ion effects and coordination environment. Additionally an f–f magnetic interaction with an 8.82 Å separation between Er^{III} ions is expected to be weak. The longest intramolecular interaction previously observed between lanthanide ions was in triple decker phthalocyanines complexes where f–f interactions were considered non-negligible up to 6.8 Å however very weak.[15a] The butterfly shape of the hysteresis curve at 1.8 K for **3** is devoid of steps, similar to $[Er^{III}(COT)_2]^-$, thus confirming the largely single-ion nature of the relaxation.

The 12 K blocking temperature observed in both **1** and **3** is the highest yet observed for a nonradical bridged SMM. Moreover the second highest observed for any SMM. The 4 K increase in the magnetic blocking of **1** over the mononuclear analogue is very substantial and suggests that extending this building block methodology to include more decks could lead to even higher blocking temperatures, bringing SMMs closer to practical working temperatures for technology applications.

Ac susceptibility measurements were performed to gain insight into the relaxation dynamics of **1** and **3** using a 3 Oe oscillating ac field. Temperature- and frequency-dependent in-phase (χ') and out-of-phase (χ'') magnetic susceptibility signals were observed for both **1** and **3** under 0 Oe applied dc field (Figures 4, S12–S13). For **1** a frequency-dependent χ'' signal

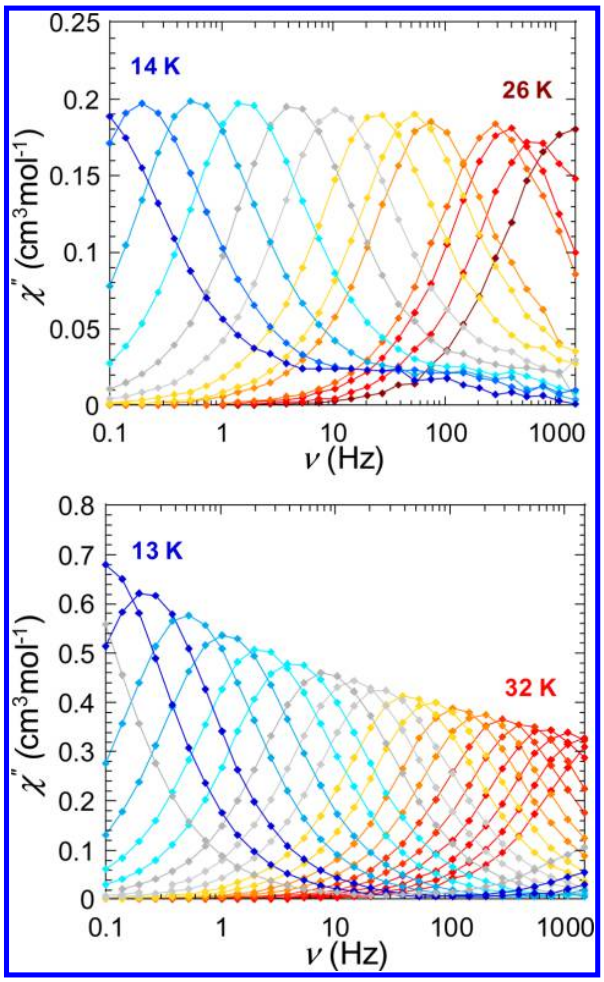

Figure 4. Out-of phase magnetic susceptibility of **1** (top) and **3** (bottom) under a zero-applied dc field between indicated temperatures.

was observed from 26 to 14 K with shifting peak maxima toward lower temperatures, indicating SMM behavior. This relaxation data fit well to the Arrhenius equation to yield an effective energy barrier (U_{eff}) of 323(3) K (231 cm^{-1}), with a pre-exponential factor of $\tau_0 = 5.7 \times 10^{-10}$s (Figure S14). The energy barrier, also called the anisotropic barrier, is the amount of energy required for reversal of the magnetization and τ_0 represents the average relaxation time in response to thermal fluctuations.[2b] The U_{eff} value and blocking temperature are often used to evaluate the success of an SMM. Not only is the energy barrier for **1** among the highest reported for an SMM but noteworthy, it is significantly higher than the 187(1) K (134 cm^{-1}) barrier observed in $[Er^{III}(COT'')_2]^-$. When the Arrhenius data were extrapolated to low temperature, the relaxation time was 100 s at 12.5 K. Solution studies of **1** show slightly enhanced ac susceptibility dynamics, consistent with dc measurements, with an effective energy barrier of 335(13) K (239 cm^{-1}) with a $\tau_0 = 1.9 \times 10^{-10}$s (Figures S15–S16).

A frequency-dependent χ'' signal was observed for **3** with shifting peak maxima toward lower temperatures confirming **3** is also an SMM. Using χ'' peak maxima between 32 and 13 K

dx.doi.org/10.1021/ja5022552 | J. Am. Chem. Soc. 2014, 136, 8003–8010

(Figure 4) and the Arrhenius law, an effective energy barrier of 306(1) K (219 cm^{-1}) with a $\tau_0 = 5.0 \times 10^{-9}$s (Figure S17) was obtained. Again this shows an increase over $[Er^{III}(COT)_2]^-$ (U_{eff} = 286 K (204 cm^{-1}), τ_0= 3.7 × 10^{-9}s) consistent with hysteresis data. When the Arrhenius data were extrapolated to low temperature, the relaxation time was 100s at 12.9 K. The frequency-dependent data for **3** indicates only **1** relaxation process is occurring between 32 and 12 K, this is surprising due to the large Er−Er separation. At such a distance we would expect each Er atom in **3** to have a unique magnetic relaxation, especially considering they are crystallographically dissimilar. To investigate the ac susceptibility of **3** over a larger temperature range, temperature-dependent studies were conducted between 32 and 1.8 K (Figure S18). The temperature-dependent χ'' signal reveals two relaxation processes occurring at approximately 7−12 and 19−32 K. The lower temperature relaxation was not observed in the lower frequency-dependent studies due to the frequency limit of the instrument. The two magnetic relaxation processes observed in temperature-dependent studies exhibit spin reversal barriers of 170(2) K (121 cm^{-1}) and 293(7) K (209 cm^{-1}). The difference in energy barrier of the two relaxations most likely arises from the two crystallographically different Er sites (see Synthesis and Structural Analysis section). Overall in both complexes **1** and **3**, coupling and crystal field environment leads to an increase in the effective energy barrier compared to their mononuclear building blocks. Interestingly, the increase in magnetic performance in the Er system is much more significant than in the Dy analogue due to strong axiality of the magnetic anisotropy. To validate our observations we performed ab inito calculations on **1** and **3** (*vide infra*).

Ab Initio Calculations and Simulations of Magnetism. Ab initio calculations of CASSCF/RASSI/SINGLE_ANISO type[16] (see the SI for computational results and details) reveal that the ground and first excited Kramers doublets on all Er^{III} sites in **1** and **3** are magnetically extremely axial, similar to what was found in the $[Er^{III}(COT)_2]^-$ monomer.[3b] The reason for strong magnetic axiality of Er^{III} ions[3b] is the negative sign of the main crystal field parameters B_2^0 and B_4^0, which leads to the stabilization of the Kramers doublet $|\pm 15/2\rangle$, with the projection of angular moment on the symmetry axis of the $[Er^{III}(COT)_2]^-$ unit in the ground state. Moreover, the main magnetic axis of the first excited Kramers doublet is almost parallel to the main magnetic axis of the ground state (Tables S6, S13). These axes at different Er sites are almost parallel to each other (Figure 5) which imply a ferromagnetic dipole−dipole interaction between the magnetic moments on these sites (Figure S21). Since the distance between Er ions in **1** is nearly twice smaller than in **3** (Figure 1), the dipole−dipole interaction in the latter is nearly eight times weaker. In fact, the reduction is even larger due to an appreciable angle between the magnetic axes on Er sites in **3**.

Broken symmetry DFT calculations for **1** (Tables S17, S19) reveal a strong antiferromagnetic exchange interaction between Er sites, significantly overcoming the ferromagnetic dipolar interaction. The same type of calculations confirms the negligible value of the exchange interaction in **3**. The calculations testify that the obtained strong antiferromagnetic coupling between Er^{III} ions in **1** is promoted effectively by the delocalized π_z orbitals of the central COT^{2-} ligand. In fact, due to noncollinearity of the main magnetic axes of Er^{III} ions in **1** (the relative angle ≈4.2°, see Figure 5 and Table S8), the ground exchange doublet has a small magnetic moment of

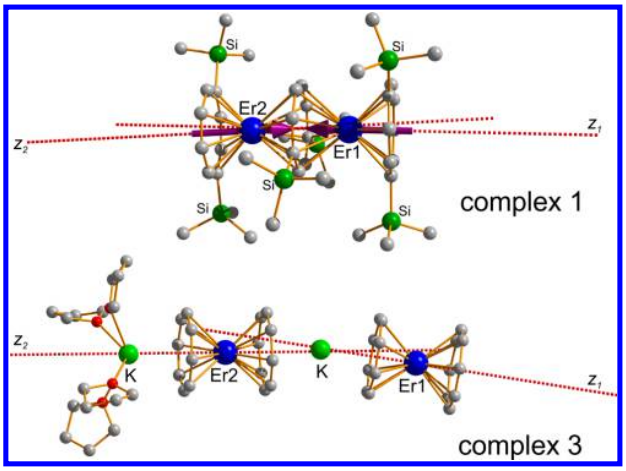

Figure 5. Red dashed lines represent the main magnetic axes of the ground Kramers doublets on Er^{III} ions in **1** (top) and **3** (bottom). Purple arrows show the strong antiferromagnetic coupling of the Er^{III} ions in **1**. In contrast to **1**, the large distance between Er ions in **3** significantly lowers the magnetic interaction, making the sites effectively uncoupled at the lowest experimental temperature (Table S18).

~0.62 μ_B (see Table S19). This is in agreement with the small slope of the magnetization curve at fields below 1.5 T (Figures 3 and S5). The first excited exchange doublet corresponds to ferromagnetic coupling of the magnetic moments, having a large value of the magnetic moment of ~17.94 μ_B. The clear step in the magnetization curve, seen at ~1.5 T, is due to level crossing of the ground and first excited exchange state (Figure 6). We notice that the hysteresis is significantly enlarged in this

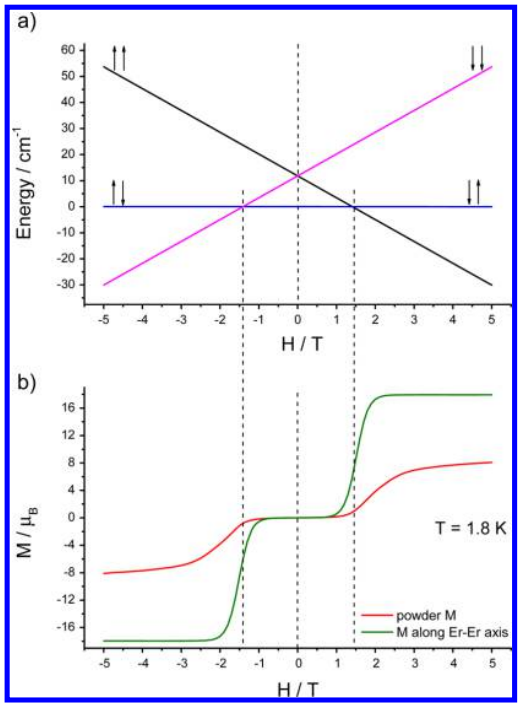

Figure 6. (a) Evolution of low-lying exchange energy states in **1** in an applied magnetic field along Er−Er axis. At fields ≈1.5 T the excited state holding the largest magnetic moment becomes the ground state, causing a steep rise of the molar magnetization (b) (cf. Figures 3a, S6).

dx.doi.org/10.1021/ja5022552 | J. Am. Chem. Soc. 2014, 136, 8003−8010

region (Figure 3, top). Since both the ground and excited exchange doublets in **1** can efficiently block the magnetization, the hysteresis loops display distinct regions corresponding to each of them being in the ground state (Figure 3).

In contrast to **1**, the significantly larger distance between Er ions in **3** dramatically reduces the magnetic interaction, both exchange and dipolar, leading to much smaller energy splitting between the ground and first excited exchange Ising doublets, of ~0.20 cm^{-1} (Table S18). This means that even at the lowest temperature achieved in experiment (1.8 K) the two $[Er^{III}(COT)_2]^-$ units are magnetically decoupled. In this temperature regime, neighboring magnetic centers act on each other merely as sources of fluctuating magnetic field resulting in the increase of the relaxation rate at each of them.[17] The same effect of the surrounding molecules is expected to enhance magnetic relaxation in the (undiluted) mononuclear $[Er^{III}(COT)_2]^-$ compound. The increased magnetic blocking observed in **3** can be attributed to the different crystal packing compared to the mononuclear $[Er^{III}(COT)_2]^-$ compound, leading to a smaller effect of the random magnetic field created by the crystal environment.

CONCLUSIONS

Two dinuclear Er^{III}−COT/COT′′ complexes were successfully isolated and structurally and magnetically investigated in detail. Both complexes exhibit remarkably large blocking temperatures and display magnetic hysteresis up to 12 K. Frozen solution measurement reveals slight improvement in the hysteresis, where openings at $H \neq 0$ are observed up until 14 K for **1**. Such magnetic performances have never been observed in any nonradical based SMMs. Both complexes show an increase in magnetic blocking properties compared to the mononuclear precursors. In **1**, the reason for the increase of SMM properties is due to the additional blocking mechanism coming from the exchange interaction between the Er sites. In **3**, the enhancement of SMM properties compared to the $[Er^{III}(COT)_2]^-$ precursor is arising from single-ion origin and a slight change in crystal field. Furthermore, the isotropic Gd analogue was synthesized and studied to probe the nature and the strength of magnetic interactions between lanthanide ions. This study confirms the exchange interaction in **3** is negligible compared to the observed interactions in **1**. The use of an aromatic bridging COT′′ ring provides a non-negligible Er−Er superexchange interaction in **1** similar to the Dy analogue.[6] Therefore, coupling spin of the SMM, while maintaining a similar crystal field around each spin carrier, resulted in an increased blocking temperature in **1**. Therefore, the 4 K increase in the magnetic blocking of **1** over the $[Er^{III}(COT'')_2]^-$ monomer may have significant implications in the field of molecular magnetism if this building block methodology can be extended to create larger multideck Er^{III}−COT complexes or 1-D chains. Such complexes would take advantage of higher nuclearity, therefore increasing blocking temperature via increasing the total spin of the complex. With this in mind, we are currently exploring synthetic strategies to isolate larger molecular $Er^{III}{}_nCOT''{}_m$ ($n > 2$, $m > 3$) systems. This represents a unique approach for isolating SMMs/SCMs with large blocking temperatures for magnetization reversal.

ASSOCIATED CONTENT

Supporting Information

Complete structural and computational details and cif files. This material is available free of charge via the Internet at http://pubs.acs.org.

AUTHOR INFORMATION

Corresponding Author

m.murugesu@uottawa.ca

Notes

The authors declare no competing financial interest.

ACKNOWLEDGMENTS

We thank the University of Ottawa, NSERC (Discovery and RTI grants), CFI for their financial support. L.U. is postdoc FWO and acknowledges support from INPAC and Methusalem program at KU Leuven.

REFERENCES

(1) (a) Leuenberger, M. N.; Loss, D. *Nature* **2001**, *410*, 789. (b) Ardavan, A.; Rival, O.; Morton, J. J. L.; Blundell, S. J.; Tyryshkin, A. M.; Timco, G. A.; Winpenny, R. E. P. *Phys. Rev. Lett.* **2007**, *98*, 057201. (c) Mannini, M.; Pineider, F.; Danieli, C.; Totti, F.; Sorace, L.; Sainctavit, P.; Arrio, M. A.; Otero, E.; Joly, L.; Cezar, J. C.; Cornia, A.; Sessoli, R. *Nature* **2010**, *468*, 417. (d) Urdampilleta, M.; Nguyen, N. V.; Cleuziou, J. P.; Klyatskaya, S.; Ruben, M.; Wernsdorfer, W. *Int. J. Mol. Sci.* **2011**, *12*, 6656. (e) Fahrendorf, S.; Atodiresei, N.; Besson, C.; Caciuc, V.; Matthes, F.; Blügel, S.; Kögerler, P.; Bürgler, D. E.; Schneider, C. M. *Nat. Commun.* **2013**, *4*, 2425. (f) Habib, F.; Lin, P.-H.; Long, J.; Korobkov, I.; Wernsdorfer, W.; Murugesu, M. *J. Am. Chem. Soc.* **2011**, *133*, 8830. (g) Aronica, C.; Pilet, G.; Chastanet, G.; Wernsdorfer, W.; Jacquot, J. F.; Luneau, D. *Angew. Chem., Int. Ed.* **2006**, *45*, 4659. (h) Mossin, S.; Tran, B. L.; Adhikari, D.; Pink, M.; Heinemann, F. W.; Sutter, J.; Szilagyi, R. K.; Meyer, K.; Mindiola, D. J. *J. Am. Chem. Soc.* **2012**, *134*, 13651.

(2) (a) Habib, F.; Murugesu, M. *Chem. Soc. Rev.* **2013**, *42*, 3278. (b) Woodruff, D. N.; Winpenny, R. E. P.; Layfield, R. A. *Chem. Rev.* **2013**, *113*, 5110 and references therein. (c) Layfield, R. A. *Organometallics* **2014**, *33*, 1084.

(3) (a) Le Roy, J. J.; Korobkov, I.; Murugesu, M. *Chem. Commun.* **2014**, *50*, 1602. (b) Ungur, L.; Le Roy, J. J.; Korobkov, I.; Chibotaru, L. F.; Murugesu, M. *Angew. Chem., Int. Ed.* **2014**, *53*, 1. (c) Jiang, S.-D.; Wang, B.-W.; Sun, H.-L.; Wang, Z.-M.; Gao, S. *J. Am. Chem. Soc.* **2011**, *133*, 4730. (d) Meihaus, K. R.; Long, J. R. *J. Am. Chem. Soc.* **2013**, *135*, 17952. (e) Liu, J.-L.; Chen, Y.-C.; Zheng, Y.-Z.; Lin, W.-Q.; Ungur, L.; Wernsdorfer, W.; Chibotaru, L. F.; Tong, M. L. *Chem. Sci.* **2013**, *4*, 3310.

(4) (a) Rinehart, J. D.; Fang, M.; Evans, W. J.; Long, J. R. *J. Am. Chem. Soc.* **2011**, *133*, 14236. (b) Demir, S.; Zadrozny, J. M.; Nippe, M.; Long, J. R. *J. Am. Chem. Soc.* **2012**, *134*, 18546. (c) Jeon, I.-R.; Park, J. G.; Xiao, D. J.; Harris, T. D. *J. Am. Chem. Soc.* **2013**, *135*, 16845. (d) Meihaus, K. R.; Corbey, J. F.; Fang, M.; Ziller, J. W.; Long, J. R.; Evans, W. J. *Inorg. Chem.* **2014**, *53*, 3099.

(5) (a) Tuna, F.; Smith, C. A.; Bodensteiner, M.; Ungur, L.; Chibotaru, L. F.; McInnes, E. J. L.; Winpenny, R. E. P.; Collison, D.; Layfield, R. A. *Angew. Chem., Int. Ed.* **2012**, *51*, 6976. (b) Layfield, R. A.; McDouall, J. W.; Sulway, S. A.; Tuna, F.; Collison, D.; Winpenny, R. E. P. *Chem.−Eur. J.* **2010**, *16*, 4442. (c) Huang, W.; Dulong, F.; Wu, T.; Khan, S. I.; Miller, J. T.; Cantat, T.; Diaconescu, P. L. *Nat. Commun.* **2013**, *4*, 1448.

(6) Le Roy, J. J.; Jeletic, M.; Gorelsky, S. I.; Korobkov, I.; Ungur, L.; Chibotaru, L. F.; Murugesu, M. *J. Am. Chem. Soc.* **2013**, *135*, 3502.

(7) (a) Jeletic, M.; Lin, P.-H.; Le Roy, J. J.; Korobkov, I.; Gorelsky, S. I.; Murugesu, M. *J. Am. Chem. Soc.* **2011**, *133*, 19286. (b) Le Roy, J. J.; Korobkov, I.; Murugesu, M. *Dalton Trans.* **2014**, *43*, 2737 2014.

(8) Jeletic, M.; Perras, F.; Gorelsky, S.; Le Roy, J. J.; Korobkov, I.; Bryce, D.; Murugesu, M. *Dalton Trans.* **2012**, *41*, 8060.
(9) Sheldrick, G. M. *SADABS, Bruker AXS area detector scaling and absorption*, version 2008/1, University of Göttingen: Göttingen, Germany, 2008.
(10) Sheldrick, G. M. *Acta Crystallogr.* **2008**, *A64*, 112.
(11) (a) Xia, J.; Jin, Z.; Chen, W. *J. Chem. Soc., Chem. Commun.* **1991**, 1214. (b) Edelmann, A.; Lorenz, V.; Hrib, C. G.; Hilfert, L.; Blaurock, S.; Edelmann, F. T. *Organometallics* **2013**, *32*, 1435. (c) Lorenz, V.; Blaurock, S.; Hrib, C. G.; Edelmann, F. T. *Organometallics* **2010**, *29*, 4787.
(12) (a) Chibotaru, L. F.; Ungur, L.; Soncini, A. *Angew. Chem., Int. Ed.* **2008**, *47*, 4126. (b) Jiang, S.-D.; Wang, B.-W.; Sun, H.-L.; Wang, Z.-M.; Gao, S. *J. Am. Chem. Soc.* **2011**, *133*, 4730. (c) Rinehart, J. D.; Fang, M.; Evans, W. J.; Long, R. J. *J. Am. Chem. Soc.* **2011**, *133*, 14236. (d) Rinehart, J. D.; Fang, M.; Evans, W. J.; Long, J. *Nat. Chem.* **2011**, *3*, 538.
(13) (a) Aharen, T.; Habib, F.; Korobkov, I.; Burchell, T. J.; Guillet-Nicolas, R.; Kleiz, F.; Murugesu, M. *Dalton Trans.* **2013**, *42*, 7795. (b) Zeng, M.; Zhang, X.; Sun, X.; Chen, X. *Angew. Chem., Int. Ed.* **2005**, *44*, 3079.
(14) Lecren, L.; Wernsdorfer, W.; Li, Y.-G.; Vindigni, A.; Miyasaka, H.; Clérac, R. *J. Am. Chem. Soc.* **2007**, *129*, 5047.
(15) (a) Fukuda, T.; Kuroda, W.; Ishikawa, N. *Chem. Commun.* **2011**, *47*, 11686. (b) Katoh, K.; Asano, R.; Miura, A.; Horii, Y.; Morita, T.; Breedlovea, B. K.; Yamashita, M. *Dalton Trans.* **2014**, DOI: 10.1039/c4dt00042k.
(16) Chibotaru, L. F.; Ungur, L. *J. Chem. Phys.* **2012**, *137*, 064112.
(17) Bhunia, A.; Gamer, M. T.; Ungur, L.; Chibotaru, L. F.; Powell, K.; Lan, Y.; Roesky, P. W.; Menges, F.; Riehn, C.; Niedner-Schatteburg, G. *Inorg. Chem.* **2012**, *51*, 9589.